Lattice dynamics and structural phase transitions in the chain compounds TMMC and TMCC. II. Raman scattering and ultrasonic measurements

1990 J. Phys.: Condens. Matter 2 8229

(http://iopscience.iop.org/0953-8984/2/42/002)

J. Phys.: Condens. Matter 2 (1990) 8229–8242. Printed in the UK

Lattice dynamics and structural phase transitions in the chain compounds TMMC and TMCC: II. Raman scattering and ultrasonic measurements

M N Braud†, M Couzi‡, N B Chanh† and A Gomez-Cuevas§

† Laboratoire de Cristallographie et de Physique Cristalline (URA 144, CNRS), Université de Bordeaux I, 33405 Talence Cédex, France

‡ Laboratoire de Spectroscopie Moléculaire et Cristalline (URA 124, CNRS), Université de Bordeaux I, 33405 Talence Cédex, France

§ Departamento de Fisica de la Matiera Condensada, Facultad de Ciencias, Universidad del Pais Vasco, Apartado 644, 48080 Bilbao, Spain

Received 10 April 1990, in final form 11 June 1990

Abstract. The structural phase transitions occurring in the chain compounds $(CH_3)_4NMnCl_3$ (TMMC) and $(CH_3)_4NCdCl_3$ (TMCC) are studied by means of Raman scattering and ultrasonic measurements. The Raman spectra recorded in the different structural modifications are fully understood on the basis of the structural data previously established in paper I. In addition, these data provide useful information on the transition mechanisms, which are of complex nature. Generally, these mechanisms involve order–disorder processes due to the reorientations of the $(CH_3)_4N^+$ groups (TMA) coupled with a displacive contribution coming from the MCl_3 octahedra chains (rotatory and translatory soft modes). The ultrasonic measurements clearly show that the I $\leftrightarrow$ III phase transition ($P6_3/m$ ($Z = 2$) $\leftrightarrow P2_1/m$ ($Z = 2$)) is 'pseudo-proper' ferroelastic, as well as the I $\leftrightarrow$ II ($P6_3/m$ ($Z = 2$) $\leftrightarrow P2_1/b$ ($Z = 4$)) transition; this latter should be of the 'trigger' type, in order to account for the unit-cell doubling.

1. Introduction

In the preceding paper (I) of this series [1], the structural phase transitions occurring in crystals of TMMC ($(CH_3)_4NMnCl_3$) and TMCC ($(CH_3)_4NCdCl_3$) have been investigated by means of x-ray diffraction and diffuse scattering experiments. We have gained much information on the space groups of the different phases, and on the nature of structural disorders due to the $(CH_3)_4N^+$ (TMA) group orientations and to the MCl_3 octrahedra chains in the high-temperature phases. However, as is well known, the diffraction methods provide a static description of the structures, and so prevent any conclusions being drawn on the driving forces responsible for the observed phase transitions. Thus, the purpose of the present paper (II) is to study the dynamical aspects of these transitions, by means of Raman scattering and ultrasonic measurements.

First, let us recall the main conclusions deduced from the preceding structural studies [1]. All structural modifications of TMMC and TMCC derive from a parent phase (I'), stable at high temperature, with space group $P6_3/mmc$ and $Z = 2$ formula units in the primitive unit cell. Another hexagonal phase (I) is stable at room temperature, with

0953-8984/90/428229 + 14 $03.50

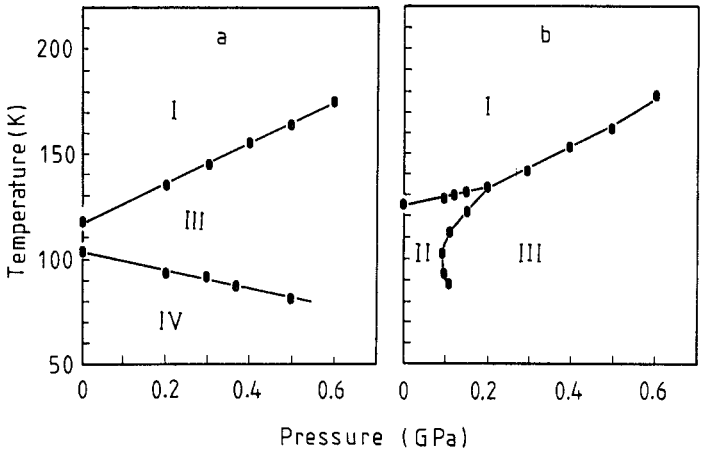

Figure 1. The P, T phase diagram of TMCC (*a*) and TMMC (*b*), as established from Raman scattering experiments [6].

space group $P6_3/m$ ($Z = 2$). Both phases I′ and I exhibit orientational disorder of the TMA, of complex nature, coupled to translational disorder of the MCl_3 octahedra chains these phenomena have been studied in detail in phase I [1]. At low temperature, ordering processes take place [2, 3] inducing different ordered phases. In the case of TMMC at zero pressure, a phase transition connects phase I to an ordered phase II with monoclinic symmetry (space group $P2_1/b$ with $Z = 4$); phase II is related to phase I by a doubling of the lattice period along the ***b*** axis, perpendicular to the sixfold axis [1]. With TMCC, two successive phase transitions occur at low temperature, leading to phase III (space group $P2_1/m$ with $Z = 2$) and then to phase IV (space group $P2_1/b$ with $Z = 12$); the complex unit cell of phase IV is related to that of phase I by a doubling of the lattice period along the ***b*** axis, together with a trebling of the period along ***c*** [1].

The structural phase transitions of TMMC and TMCC have already been the subject of numerous investigations by means of Raman scattering experiments [3–6]. In particular, the P, T phase diagrams of these materials (figure 1) have been established [6], showing that phase III becomes stable in TMMC at low temperature, for pressures higher than ~0.1 to 0.2 GPa. In both TMMC and TMCC, the Raman spectra of phase I are well understood on the basis of the selection rules derived from $P6_3/m$ space group with $Z = 2$ [4]. The I ↔ II phase transition of TMMC observed at zero pressure (figure 1(*b*)) was first analysed [4, 5] according to a pure order–disorder model related to the TMA orientations [3], and so it was concluded that the unit cell of phase II, if monoclinic, should contain more than four formula units [5]. More recently [6], in the light of inelastic neutron scattering data [7], it has been pointed out that the low-frequency Raman spectra of phase II could be reconciled with space group $P2_1/b$ ($Z = 4$) as well, provided that the I ↔ II transition is induced by anti-phase translational displacements of the octahedra chains along the ***c*** axis. Indeed, the structural data reported in paper I [1] are in full agreement with the latter point of view. In the case of TMCC, the Raman spectra of phase III are consistent with an ordered structure with space group $P2_1/m$ ($Z = 2$) [6], whereas the complex vibrational features observed in phase IV [4, 5], in retrospect, agree with the large unit cell ($P2_1/b$ with $Z = 12$) as reported in paper I [1].

It has been emphasized in paper I [1] that hexagonal ↔ monoclinic phase transitions, as observed in TMMC and TMCC, are ferroelastic since they involve a change of the

crystalline system; as a result, the monoclinic phases exhibit domain structures as evidenced on Weissenberg photographs [1]. Thus, it is important in such cases to study the behaviour of the elastic constants associated with the strain tensor components that can couple with the order parameter of the transition. Indeed, Brillouin scattering experiments have been performed with both TMMC [8] and TMCC [9], showing anomalies in the temperature dependence of the C_{11} and C_{33} elastic constants at the transition temperatures. However, the $C_{66} = \frac{1}{2}(C_{11} - C_{12})$ elastic constant (hexagonal system) should be much more informative in the analysis of the transition mechanism, since C_{66} is associated with the $(e_1 - e_2, e_6)$ strain tensor components, which represent an order parameter for the hexagonal $\leftrightarrow$ monoclinic transformation. In fact, C_{66} could not be accurately measured by means of Brillouin scattering, due to the very low scattering cross section associated with the corresponding transverse acoustic mode [8].

Thus, the aim of the present paper is first to complement the previous Raman scattering data. The experiments reported here are focused on the study of the I′ $\leftrightarrow$ I phase transition, which has not been reported before [3–6], and on the temperature dependence of the E_{2g} spectrum, which corresponds to the symmetry of the order parameter for the hexagonal $\leftrightarrow$ monoclinic transformations (see section 3). The behaviour of the translatory mode of the octahedra chains will be more precisely analysed, since it has been shown recently to play an important role in the mechanism of the I $\leftrightarrow$ II phase transition [1]. On the other hand, the temperature dependence of the C_{11} and C_{66} elastic constants of TMMC, as measured through the phase transitions using the ultrasonic technique, will be reported.

2. Experimental details

Sample preparation has been described previously [1]. Single crystals of TMMC and TMCC with dimensions up to $3 \times 3 \times 8$ mm^3 have been used for Raman scattering experiments. The large TMMC single crystal of size $8 \times 5 \times 5$ mm^3 used for ultrasonic measurements was a gift from Dr J P Renard (Institut d'Electronique Fondamentale, Université Paris-Sud, Orsay).

The Raman spectra have been recorded with either a Dilor Z24 triple monochromator or a Jobin-Yvon Ramanor HG2S double monochromator instrument, coupled with Spectra-Physics argon ion lasers model 171 and 164, respectively. For the colourless TMCC crystals, the 514.5 or 488.0 nm emission lines have been used indifferently, but in the case of the pink TMMC crystals, only the 488.0 nm line gave detectable Raman scattering signals. Low-temperature experiments, down to ~20 K, have been made with a Cryodine model 20 helium refrigerator, equipped with the sample holder modification described in [10]. Combined high-pressure (up to ~0.6 GPa) and low-temperature (down to ~80 K) measurements were performed with the home-made device described in [11].

Ultrasonic measurements have been performed using Matec equipment, a model 6600 pulse generator. The transit time of the ultrasonic pulses was measured by the pulse–echo overlap method [12]. Coaxially gold-plated *X*- and *Y*-cut quartz transducers of fundamental frequency 10 MHz were used to generate longitudinal and shear modes, respectively. Transducers were bonded to the crystal with Dow resin 276-V9 for measurements near room temperature and with Nonaq stopcock grease for low temperatures. A liquid nitrogen cryostat from Air-Products has been used for low-temperature experiments. The ultrasonic wave velocities were calculated from the overlap frequencies

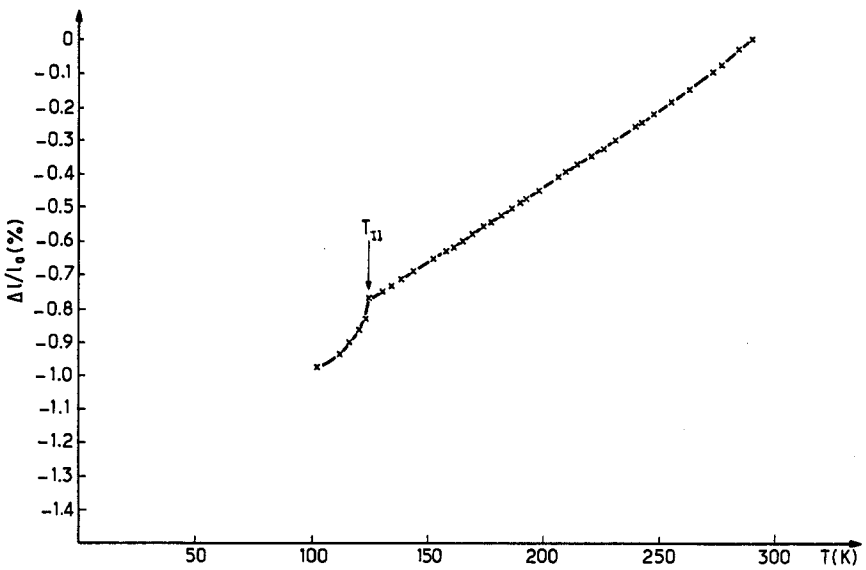

Figure 2. The thermal expansion of TMMC single crystal in a direction perpendicular to the hexagonal *c* axis (l_0 = 4.38 mm).

using sample lengths corrected from thermal expansion; to do this, the thermal expansion was measured between room temperature and ~100 K (figure 2) with a Perkin-Elmer dilatometer TMS1 (sensitivity 10^{-4} mm mm^{-1}).

3. Group theory of lattice dynamics and phase transitions

3.1. Lattice vibrations

The low-frequency part of the Raman spectra (0–300 cm^{-1}) corresponds to the so-called 'lattice vibrations', including all vibrational modes of the octahedra chains and the external (translatory and rotatory) vibrations of the TMA groups [4]. From classical factor-group analysis [13], the enumeration of the zone-centre ($\boldsymbol{k} = 0$) lattice vibrations in the parent phase I′ is found:

$$\Gamma_{\text{lattice}} = A_{1g} + 2A_{2g} + 2B_{1g} + 2E_{1g} + 3E_{2g} + 3A_{2u} + 2B_{1u} + 2B_{2u} + 4E_{1u} + 3E_{2u}.$$

This enumeration includes the three acoustic modes ($A_{2u} + E_{1u}$) of zero frequency at $\boldsymbol{k} = 0$. The modes with even (g) symmetry can be described as follows [4, 14]:

(i) The totally symmetric A_{1g} mode corresponds to the in-phase elongation of all M–Cl bonds: it is the 'breathing' mode of the octahedra chains.

(ii) The two A_{2g} modes correspond respectively to a rotatory mode of the octahedra chain as a whole around the hexagonal axis, and to a rotatory vibration of the TMA groups around the same axis.

(iii) The B_{1g} representation contains an 'accordion' mode of the octahedra chains, in which successive planes of Cl atoms move out of phase along the hexagonal axis, and a translatory vibration of the TMA along the same axis.

Table 1. Compatibility relations for the zone-centre lattice vibrations in TMMC and TMCC through the I′ ↔ I ↔ III phase sequence.

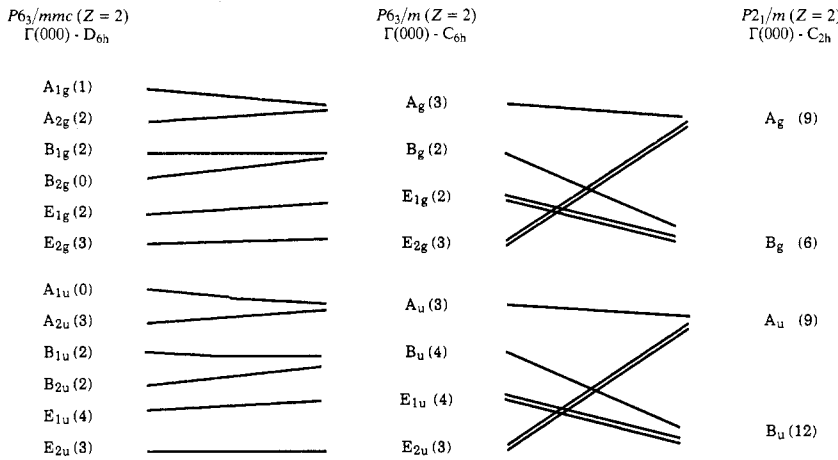

(iv) The two E_{1g} modes are respectively an internal deformation of the octahedra chains and a degenerate rotatory mode of the TMA around axes perpendicular to the sixfold axis.

(v) Finally, the three E_{2g} modes can be described as two internal deformations of the octahedra chains and one degenerate translatory vibration of the TMA perpendicular to the hexagonal axis.

In phase I′, only A_{1g} ($\alpha_{xx} + \alpha_{yy}$, α_{zz}), E_{1g} (α_{xz}, α_{yz}) and E_{2g} ($\alpha_{xx} - \alpha_{yy}$, α_{xy}) vibrations are Raman-active [15].

Phases I′, I and III exhibit the same unit-cell volume ($Z = 2$), which means that all phase transitions between these different structural modifications occur at the centre (Γ point) of the Brillouin zone. Then, the determination of compatibility relations for the zone-centre lattice modes in these phases is straightforward, as shown in table 1. It is worth noting that the inactive A_{2g} modes in phase I′ become Raman-active in phase I and in phase III ($A_{2g} \rightarrow A_g$ ($\alpha_{xx} + \alpha_{yy}$, α_{zz}) $\rightarrow A_g$ (α_{xx}, α_{yy}, α_{zz}, α_{xy})) while the inactive B_{1g} modes (I′) remain inactive in phase I but become Raman-active in phase III ($B_{1g} \rightarrow B_g \rightarrow B_g$ (α_{xz}, α_{yz})). On the other hand, the degenerate E_{1g} and E_{2g} modes of phases I′ and I are expected to be split into two components in phase III ($E_{1g} \rightarrow 2B_g$, $E_{2g} \rightarrow 2A_g$). The correlation diagrams of table 1 also show that the order parameter for the I′ ↔ I transition has the A_{2g} symmetry and that for the I ↔ III transition the E_{2g} symmetry.

The compatibility relations for the I ↔ II transition (table 2) must take into account the unit-cell doubling occurring in phase II, which replaces point M ($0\,\frac{1}{2}\,0$) of the hexagonal Brillouin zone [16] at zone centre in phase II. Then the zone-centre modes in phase II must be correlated with those of phase I and with the zone-boundary modes at point M. It should be noticed that both representations M_2^+/B_g and M_1^-/A_u induce the $P2_1/b$ space group [17]. In table 2, the M_1^-/A_u representation has been chosen because it corresponds to the symmetry of the transverse acoustic mode TA(M) (anti-phase translational displacements of the octahedra chains along the *c* axis), which is related to

Table 2. Compatibility relations for the zone-centre lattice vibrations in TMMC through the I′ ↔ II phase transition.

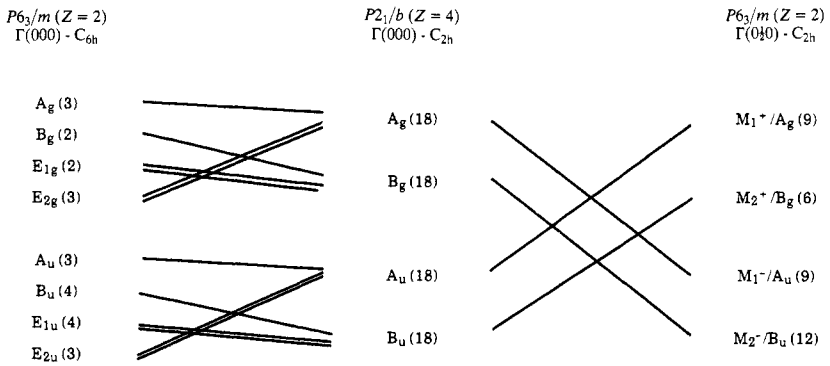

an order parameter for this transition [1, 6, 7]. It is worth noting that the E_{2g} representation also induces the unity representation in space group $P2_1/b$ (table 2), which means that E_{2g} should be associated with another order parameter. In section 5 it will be shown that E_{2g} actually corresponds to the primary order parameter, while the M_1^-/A_u is a 'triggered' one.

The correlation diagrams for the III ↔ II phase transition can be easily obtained by combining tables 1 and 2.

In phase IV, because of cell doubling along ***b*** together with a trebling along ***c***, points U ($0\ \frac{1}{2}\ \alpha$) and $\bar{\text{U}}$ ($0\ \frac{1}{2}\ \bar{\alpha}$) of the hexagonal Brillouin zone [16] (with $\alpha = \frac{1}{3}$) are replaced at zone centre, in addition to the point M defined above. It is not meaningful to give here such a complex correlation diagram; note however that the enumeration of $\boldsymbol{k} = 0$ lattice vibrations in phase IV ($P2_1/b$ with $Z = 12$) is the following:

$$\Gamma_{\text{lattice}} = 54\,A_g + 54\,B_g + 54\,A_u + 54\,B_u.$$

3.2. Pseudo-spin coordinates

In order to account for the order–disorder processes due to TMA reorientations, which are connected to the transition mechanisms, we shall consider a multidimensional pseudo-spin model, of which the general formulation has been presented in detail elsewhere [18]. Indeed, orientational disorder of the TMA in phase I can be described by a complex Frenkel-type model (see paper I [1]) corresponding to an admixture of a model (1) and of a model (2) associated with two and three energetically equivalent potential wells, respectively. Let us call $\bar{\theta}_i$ the mean occupation probability for a given TMA in the orientation i; the index values $i = 1, 2$ refer to the two mirror-related orientations found in model (1) and $i = 3, 4, 5$ to the three potential wells associated with model (2). Then in phase I one has [1]

$$\begin{aligned} \bar{\theta}_1 &= \bar{\theta}_2 = \tfrac{1}{2}p_1 \\ \bar{\theta}_3 &= \bar{\theta}_4 = \bar{\theta}_5 = \tfrac{1}{3}p_2 \end{aligned} \qquad (1)$$

where p_1 and p_2 are the relative weights of models (1) and (2) ($p_1 + p_2 = 1$).

The symmetry-breaking pseudo-spin coordinates issued from the models (1) and (2) can be written [6, 14]:

$$\begin{aligned}\Theta(1) &= (1/\sqrt{2})(\bar{\theta}_1 - \bar{\theta}_2)\\ \Theta(2) &= (1/\sqrt{6})(2\bar{\theta}_3 - \bar{\theta}_4 - \bar{\theta}_5)\\ \Theta(3) &= (1/\sqrt{2})(\bar{\theta}_4 - \bar{\theta}_5)\end{aligned} \tag{2}$$

with $(\bar{\theta}_1 + \bar{\theta}_2) = p_1$ and $(\bar{\theta}_3 + \bar{\theta}_4 + \bar{\theta}_5) = p_2$.

Since the primitive unit cell contains two TMA groups (phase I), each one of these coordinates gives rise to two different branches in the Brillouin zone [18]. So, at the zone centre (Γ point) $\Theta(1)$ induces the B_g and A_u representations while $\Theta(2)$ and $\Theta(3)$ are degenerate in pairs according to the E_{2g} and E_{1u} representations (complex conjugate representations). At the zone boundary point M ($0\,\frac{1}{2}\,0$), $\Theta(1)$ induces the representations M_2^+/B_g and M_1^-/A_u while $\Theta(2)$ and $\Theta(3)$ transform according to $2M_1^+/A_g + 2M_2^-/B_u$ [6].

Thus, the $\Theta^{(1)}_{M_1^-}$ and/or $\Theta^{(2)}_{E_{2g}}$, $\Theta^{(3)}_{E_{2g}}$ coordinates may act as order parameters for the I $\leftrightarrow$ II and I $\leftrightarrow$ III phase transitions, since they belong to the correct symmetry type.

In order to describe the I′ $\leftrightarrow$ I phase transition in such a way, one has to take into account the additional vertical mirror plane (σ_v) that appears in space group $P6_3/mmc$ (phase I′). As a result, all potential wells of models (1) and (2) as defined in phase I must be split into two mirror-related (σ_v) energetically equivalent orientations in phase I′. Let us call $\bar{\theta}'_i$ the occupation probabilities of the TMA in such new orientations. Then, in phase I′ one has

$$\bar{\theta}_1 = \bar{\theta}_2 = \bar{\theta}'_1 = \bar{\theta}'_2 = \tfrac{1}{4}p_1$$
$$\bar{\theta}_3 = \bar{\theta}_4 = \bar{\theta}_5 = \bar{\theta}'_3 = \bar{\theta}'_4 = \bar{\theta}'_5 = \tfrac{1}{6}p_2.$$

Now, the I′ $\leftrightarrow$ I phase transition can be associated with two pseudo-spin coordinates belonging to the A_{2g} representation at zone centre (symmetry of the order parameter), namely

$$\begin{aligned}\Theta'^{(1)}_{A_{2g}} &= (1/2)(\bar{\theta}_1 + \bar{\theta}_2 - \bar{\theta}'_1 - \bar{\theta}'_2)\\ \Theta'^{(2)}_{A_{2g}} &= (1/\sqrt{6})(\bar{\theta}_3 + \bar{\theta}_4 + \bar{\theta}_5 - \bar{\theta}'_3 - \bar{\theta}'_4 - \bar{\theta}'_5)\end{aligned} \tag{3}$$

with

$$\bar{\theta}_1 + \bar{\theta}_2 + \bar{\theta}'_1 + \bar{\theta}'_2 = p_1$$

and

$$\bar{\theta}_3 + \bar{\theta}_4 + \bar{\theta}_5 + \bar{\theta}'_3 + \bar{\theta}'_4 + \bar{\theta}'_5 = p_2.$$

The coordinates (3) lead to the phase I ground state as defined by the relations (1).

4. Raman scattering

First, let us recall that the low-frequency Raman spectra of TMMC and TMCC in phase I have been well interpreted [4] according to the group-theoretical predictions given in section 3.1. The three expected A_g modes are observed respectively at $\simeq 250\,cm^{-1}$ ('breathing' mode of the octahedra chains), $\simeq 80\,cm^{-1}$ (rotatory mode of the chain)

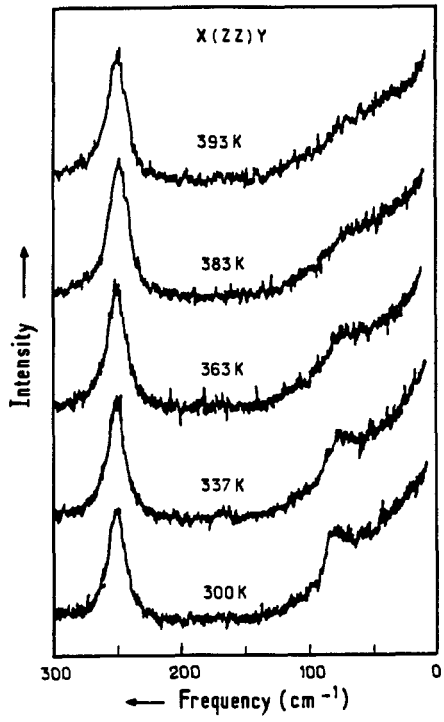

Figure 3. Temperature dependence of the $A_{1g} \rightarrow A_g(\alpha_{zz})$ Raman spectrum of TMMC through the I′ ↔ I phase transition at zero pressure (T_1 = 389 K).

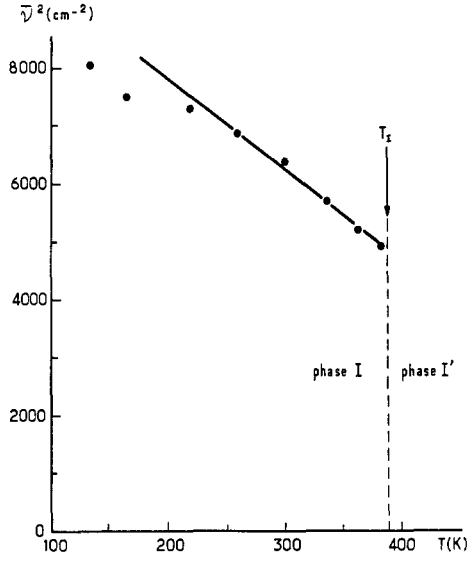

Figure 4. Temperature dependence of the square of the chain rotatory mode frequency.

and ≃50 cm^{-1} (TMA libration). Note that the latter is observed only on the α_{zz} spectrum and appears as a large signal centred on the Rayleigh line, resembling the response function of an overdamped oscillator [3, 4]. The three expected E_{2g} modes are observed respectively at ≃170 and ≃120 cm^{-1} (internal deformations of the chains) and at ≃80 cm^{-1} (TMA translatory). As for the E_{1g} spectra, they are featureless in the case of TMCC but reveal a weak line at ≃120 cm^{-1} with TMMC, assigned to a chain mode [4].

4.1. The I′ ↔ I phase transition

According to table 1, no modification is observed in the E_{1g} and E_{2g} spectra of both TMMC and TMCC when going from phase I to phase I′ at high temperature. In contrast, changes are expected to occur in the A_g spectrum, since two Raman-active A_g modes of phase I (chain rotatory and TMA libration) become Raman-inactive with A_{2g} symmetry in phase I′ (table 1).

Figure 3 shows the temperature dependence of the A_g (α_{zz}) spectrum of TMMC, through the I′ ↔ I phase transition. As expected, the breathing mode of the chain at ≃250 cm^{-1} is still present in phase I′ ($A_g \rightarrow A_{1g}$) and the chain rotatory mode at ≃80 cm^{-1} progressively disappears ($A_g \rightarrow A_{2g}$); the decrease in intensity of this mode is accompanied by a slight softening of its frequency (figure 4). Another striking feature observed is the persistence of the low-frequency broad signal in phase I′ (figure 3).

As mentioned already, the low-frequency signal if assigned to an overdamped TMA libration with A_g symmetry should disappear in phase I' ($A_g \rightarrow A_{2g}$). This is clearly not the case, and more likely this feature has to be assigned in both phases I and I' to disorder-induced scattering. Now, as established in paper I [1], structural disorder comes not only from the TMA reorientations but also from the octahedra chains, which perform anisotropic disordered translational displacements along the z axis. Because the 'Rayleigh wing' appears only on the α_{zz} spectrum, we think that the disordered motions of the chains along z contribute to this scattering. Probably, coupling occurs between these disordering modes of the chains and TMA librations, resulting in the observation of a broad signal extending from 0 to $\simeq 100\ cm^{-1}$ (figure 3).

The softening of the octahedra chain rotatory mode observed when the transition temperature is approached from below (figure 4) is an indication of a displacive contribution in the transition mechanism, coming from chain rotation. However, at the transition temperature ($T_I = 389$ K), the frequency of the rotatory mode is far from being zero, even though the transition is of second order (or nearly second order) [1]. Such a behaviour can be explained by means of a bilinear coupling that can exist between the A_{2g} chain rotation coordinate and the pseudo-spin coordinates $\Theta'^{(1)}_{A_{2g}}$ and $\Theta'^{(2)}_{A_{2g}}$ (see section 3.2) with the same symmetry. Then, the rotatory soft-mode frequency does not tend to zero at T_I because the pseudo-spin coordinate freezes at that temperature, before the optical soft mode can do it (see paper III).

4.2. The I ↔ III phase transition

At zero pressure, phase III can be observed only with TMCC, in a narow range of temperature (figure 1(*a*)). Thus, high-pressure measurements around 0.5 GPa have been carried out, where the range of stability of phase III is much larger (figure 1). Under such conditions, phase III can be more easily characterized, and in particular it has been concluded that the structure corresponds to an ordered state of the TMA [6], in contrast with a previous erroneous statement based on zero-pressure experiments [4]. However, it should be pointed out that the use of corindon windows in the high-pressure cell [11] generally prevents the observation of accurate polarisation selections [6]. Nevertheless, the symmetry of the observed modes can be determined unambiguously by comparison with the previous data obtained at zero pressure [4].

Thus, the E_{2g} spectra (figure 5) are of particular interest, since they correspond to the symmetry of the order parameter for the I ↔ III transition. In phase III, we observe the splitting of all E_{2g} lines according to the scheme $E_{2g} \rightarrow 2A_g$ (table 1). The abrupt and discontinuous spectral changes confirm the first-order character of this transition. All expected E_{2g} modes are indeed observed, and none of them behave as a soft mode. Consequently, it can be safely stated that there exists no displacive contribution in the I ↔ III transition mechanism, so that this phase change has pure order–disorder character, owing to the $\Theta^{(2)}_{E_{2g}}$ and $\Theta^{(3)}_{E_{2g}}$ pseudo-spin coordinates that are expected to become frozen in phase III (see section 3.2).

As a matter of fact, the TMA disorder produces in phase I a noticeable broadening of all Raman lines whereas in phase III these lines become narrow and are split according to crystal-field correlations, as expected for an ordered state (figure 5). The same holds true for the internal vibrations of the TMA [4, 19]. Nevertheless, the E_{2g} pseudo-spin variables do not give rise to any detectable quasi-elastic (Rayleigh) scattering in phase I, even though the characteristic times for TMA reorientations lie in the range of 10^{-12} s [20]. Probably, this absence of quasi-elastic scattering must be related to the tetrahedral

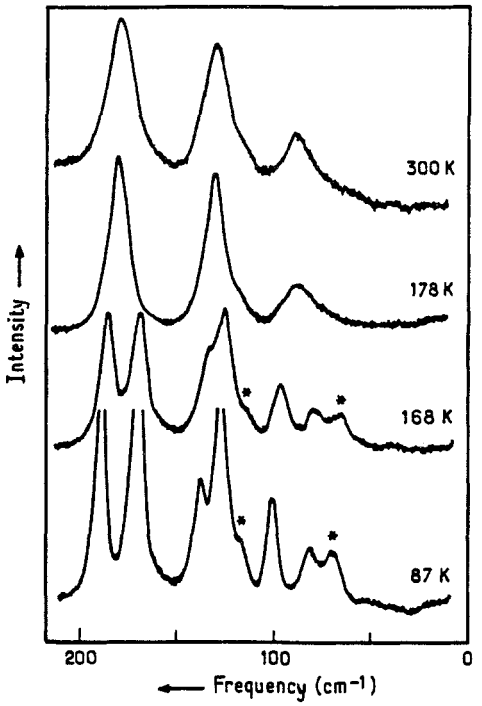

Figure 5. Temperature dependence of the $E_{2g} \rightarrow A_g$ (α_{xy}) Raman spectrum of TMMC at 0.51 GPa, through the I ↔ III phase transition (transition temperature ≈ 170 K). The asterisks indicate the presence of B_g modes (see text).

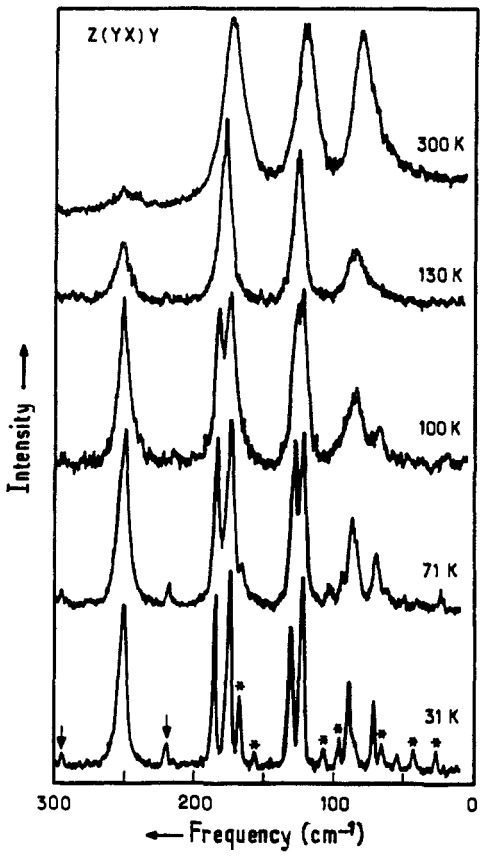

Figure 6. Temperature dependence of the $E_{2g} \rightarrow A_g$ (α_{xy}) Raman spectrum of TMMC at zero pressure, through the I ↔ II phase transition (T_{II} = 126 K). The asterisks indicate the frequencies of the zone boundary modes (M_1^-/A_u), and the arrows correspond to the internal torsional modes of the TMA ($\tau(CH_3)$).

symmetry of the TMA, whose reorientations with F_1 symmetry in the T_d point group (Raman-inactive) would not induce important variations of the crystal polarisability.

4.3. The I ↔ II phase transition

The temperature dependence of the E_{2g} Raman spectra of TMMC at zero pressure through the I ↔ II phase transition (figure 6) is in full agreement with the group-theoretical predictions given in table 2. One observes the splitting of all E_{2g} lines according to the scheme $E_{2g} \rightarrow 2A_g$, and additional lines coming from the zone boundary modes with M_1^-/A_u symmetry are clearly seen. Among these new lines, that of lowest frequency, i.e. situated at ≈25 cm^{-1} (figure 6), is unambiguously assigned to a transverse acoustic mode at point M, TA(M), after the inelastic neutron scattering results of Hutchings *et al*

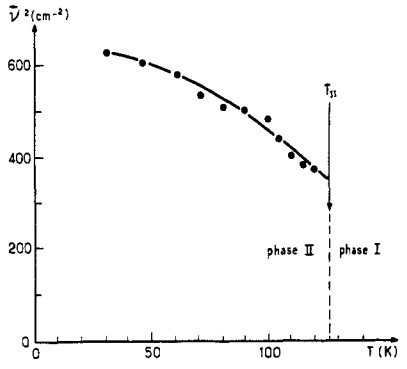

Figure 7. Temperature dependence of the square of the TA(M) translatory mode frequency.

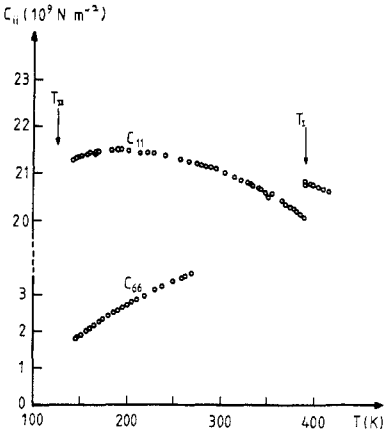

Figure 8. Temperature dependence of the C_{11} and C_{66} elastic constants of TMMC at zero pressure, through the I′ ↔ I ↔ II phase sequence.

[7]. Also, the discontinuous spectral changes observed at $T_{II} \simeq 126$ K confirm that the I ↔ II transition is of first order.

The TA(M) mode at ≃25 cm^{-1} corresponds to anti-translational displacements of the octahedra chains along the *c* axis [7]. As shown in figure 7, its frequency undergoes a marked softening when the transition temperature is approached from below. Thus, the I ↔ II transition exhibits some displacive character, due to chain translations, as expected from diffraction data [1].

The TA(M) frequency is far from being zero at T_{II}. This is explained by the fact that the I ↔ II transition is of first order and possibly also by bilinear coupling that can exist between the TA(M) mode and the $\Theta^{(1)}_{M_1^-}$ pseudo-spin coordinate of the same symmetry.

Ordering of the TMA in phase II can be achieved by means of either the $\Theta^{(1)}_{M_1^-}$ or the $\Theta^{(2)}_{E_{2g}}$ and $\Theta^{(3)}_{E_{2g}}$ pseudo-spin coordinates, which all correspond to order parameters for the phase transition (see section 3).

4.4. The III ↔ II phase transition

This transition is observed with TMMC at high pressure and low temperature (figure 1(*b*)). The results obtained show that this phase transition is also of first order, owing to the abrupt spectral changes observed. Thus, it is now clearly established that all transitions occurring between phase I, II and III around the triple point (figure 1(*b*)) are of first order.

4.5. The III ↔ IV phase transition

For the sake of completeness, let us recall that the Raman spectra of TMCC in phase IV [4] closely resemble those of TMMC in phase II, except that many more additional weak lines coming from zone-boundary modes are observed as expected for the complex unit cell $P2_1/b$ with $Z = 12$ [1] (see section 3.1).

5. Ultrasonic measurements

The study of the elastic constant $C_{66} = \frac{1}{2}(C_{11} - C_{12})$ [21] is of major interest, since it is associated with the strain components $(e_1 - e_2, e_6)$ that belong to the E_{2g} representation (order parameter).

The velocities of ultrasonic waves propagating along the [100] direction of a TMMC single crystal have been investigated at different temperatures, through the $I' \leftrightarrow I \leftrightarrow II$ phase sequence occurring at zero pressure. The longitudinal mode polarised along [100] corresponds to the C_{11} elastic constant, while the transverse mode, polarised perpendicular to [001], corresponds to C_{66} [22] ($C_{ij} = \rho v^2$, where ρ is the mass density of the crystal and v is the corresponding sound wave velocity). Unfortunately, ultrasonic echoes were lost in phase II, because of the ferroelastic domains.

The results are shown in figure 8. The temperature dependence of C_{11} in the high-temperature range is dominated by anharmonic effects due to the thermal expansion of the crystal (figure 2), which produces a monotonic (quasi-linear) increase of C_{11} with decreasing temperatures. However, one notices a well defined step-like anomaly of C_{11} at the $I' \leftrightarrow I$ transition temperature. In phase I, there is a balance between the thermal expansion effects mentioned above and a softening of C_{11} when the $I \leftrightarrow II$ transition temperature is approached from above, resulting in a maximum value for C_{11} around 200 K (figure 8). Similar results have been obtained by Levola and Laiho from Brillouin scattering experiments [8]. On the other hand, the elastic constant C_{66} exhibits a marked softening when the $I \leftrightarrow II$ transition temperature T_{II} is approached from above (figure 8). C_{66} does not tend to zero at T_{II} because of the first-order character of the transition. It should be pointed out that preliminary results obtained with TMCC show that in phase I C_{66} exhibits the same behaviour as that reported in figure 8, when approaching the transition temperature to phase III.

The temperature dependences of C_{11} and C_{66} will be analysed in detail according to a thermodynamic potential developed in the framework of Landau theory (see paper III). However, it is already possible to explain these data on qualitative grounds. So, the step-like variation of C_{11} at the $I' \leftrightarrow I$ transition temperature is characteristic of linear–quadratic coupling existing between the strain components and the order parameter [23]. Indeed, the order parameter ρ has A_{2g} symmetry (see section 3) so that $[A_{2g}]^2 = A_{1g}$, and the strain component $(e_1 + e_2)$ associated with C_{11} has A_{1g} symmetry. Then, there exists an invariant of the form $\rho^2(e_1 + e_2)$. On the other hand, the strong softening as observed for C_{66} in both TMMC and TMCC is characteristic of bilinear coupling existing between the E_{2g} strain components $(e_1 - e_2, e_6)$ and the order parameter. This means that the order parameter has E_{2g} symmetry and that both phase transitions $I \leftrightarrow II$ and $I \leftrightarrow III$ are proper (or pseudo-proper) ferroelastic.

A proper ferroelastic character is indeed expected for the $I \leftrightarrow III$ transition occurring at the zone centre, but it is unusual for the $I \leftrightarrow II$ transition involving a multiplication of the unit-cell volume. Generally, such a transition is driven by a zone-boundary order parameter (M_1^-/A_u in our case) and the zone-centre strain component acts as a secondary order parameter (improper ferroelastic transition). If such was the case in TMMC, C_{66} would remain essentially constant in phase I [23]. Thus, we are led to the conclusion that the $I \leftrightarrow II$ phase transition is of the 'trigger' type, i.e. it is driven by the zone-centre E_{2g} order parameter (primary order parameter), which triggers the zone boundary one (M_1^-/A_u), in order to account for the unit-cell doubling. Such a mechanism has been predicted by Holakovsky [24] and was evidenced experimentally for the first time by Toledano in the case of benzyl [25]. It should be pointed out that trigger-type phase

transitions are necessarily of first order [24], which is indeed the case for the I ↔ II transition of TMMC.

6. Conclusions

The structural phase transitions observed in TMMC and TMCC depend on complex mechanisms in which the order parameters generally correspond to order–disorder processes (pseudo-spin coordinates) coupled with a displacive contribution (soft modes). In addition, coupling may also exist between the order parameters and the strain tensor components (ferroelastic phase transitions).

The second-order I′ ↔ I phase transition (ferroïc–non-ferroelastic) is driven by TMA reorientations coupled with an optical soft mode due to octahedra chain rotation. It connects two different orientationally disordered phases, where the extent of disorder is higher in phase I′ than in phase I.

The I ↔ III phase transition is purely order–disorder, due to a pseudo-spin coordinate with E_{2g} symmetry coupled with the strain components of the same symmetry. This results in a 'pseudo-proper' ferroelastic phase transition. The same mechanism has been established for the I ↔ II transition, but in addition, the zone-centre E_{2g} order parameter 'triggers' a zone-boundary M_1^-/A_u acoustic phonon responsible for a displacive contribution connected with the unit-cell doubling. Thus, it is concluded that the I ↔ II phase transition is of the 'trigger' type.

It is clearly established that all transitions between phases I, II and III occurring around the triple point are of first order. Finally, the Raman spectra of phase IV are consistent with the complex unit cell $P2_1/b$ ($Z = 12$) previously determined.

Acknowledgments

The authors wish to thank Dr J P Renard (Institut d'Electronique Fondamentale, Université Paris-Sud, Orsay, France) for the gift of a large TMMC single crystal used in ultrasonic measurements. This work was supported in part by a Franco-Spanish 'Action Intégrée'. M Couzi would like to thank the 'Région Aquitaine' for providing us with a part of the Raman equipment used in this study.

References

[1] Braud M N, Couzi M, Chanh N B, Courseille C, Gallois B, Hauw C and Meresse A 1990 *J. Phys.: Condens. Matter* **2** 8209
[2] Mangum B W and Utton D B 1972 *Phys. Rev.* B **6** 2790
[3] Peercy P S, Morosin B and Samara G A 1973 *Phys. Rev.* B **8** 3378
[4] Mlik Y, Daoud A and Couzi M 1979 *Phys. Status Solidi* a **52** 175
[5] Mlik Y and Couzi M 1982 *J. Phys. C: Solid State Phys.* **15** 6891
[6] Couzi M and Mlik Y 1986 *J. Raman Spectrosc.* **17** 117
[7] Hutchings M T, Pawley G S and Stirling W G 1983 *J. Phys. C: Solid State Phys.* **16** 115
[8] Levola T and Laiho R 1986 *J. Phys. C: Solid State Phys.* **19** 6931
[9] Levola T and Laiho R 1988 *Solid State Commun.* **66** 557
[10] Cavagnat R, Cornut J C, Couzi M, Daleau G and Huong P V 1978 *Appl. Spectrosc.* **32** 500

[11] Martin J J, Cavagnat R, Cornut J C, Couzi M, Daleau G, Devaure J, Maissara M and Mokhlisse R 1986 *Appl. Spectrosc.* **40** 217
[12] Papadakis E P 1967 *J. Acoust. Soc. Am.* **42** 1045
[13] Turrell G 1972 *Infrared and Raman Spectra of Crystals* (London: Academic Press)
[14] Mlik Y 1981 *Thesis* University of Tunis
[15] Poulet H and Mathieu J P 1970 *Spectres de Vibration et Symétrie des Cristaux* (Paris: Gordon and Breach) pp 244, 245
[16] Bradley C J and Cracknell A P 1972 *The Mathematical Theory of Symmetry in Solids* (Oxford: Clarendon Press)
[17] Stokes H T and Hatch D M 1988 *The Isotropy Subgroups of the 230 Crystallographic Space Groups* (Singapore: World Scientific) p 107
[18] Couzi M, Negrier P, Poulet H and Pick R M 1988 *Croat. Chem. Acta* **61** 649
[19] Braud M N and Couzi M 1989 unpublished results
[20] Guillaume F, Couzi M and Bee M 1990 in preparation
[21] Nye J F 1963 *Propriétés Physiques des Cristaux; leur Représentations par des Tenseurs et des Matrices* (Paris: Dunod)
[22] Brugger K 1965 *J. Appl. Phys.* **36** 759
[23] Rehwald W 1973 *Adv. Phys.* **22** 721
[24] Holakovsky J 1973 *Phys. Status Solidi* b **56** 615
[25] Toledano J C 1979 *Phys. Rev.* B **20** 1147